International Journal of Plasticity 26 (2010) 976–991

Contents lists available at ScienceDirect

International Journal of Plasticity

journal homepage: www.elsevier.com/locate/ijplas

A 3-D phenomenological constitutive model for shape memory alloys under multiaxial loadings

J. Arghavani [a,1], F. Auricchio [b,c,d], R. Naghdabadi [a,e,*], A. Reali [b,d], S. Sohrabpour [a]

[a] Department of Mechanical Engineering, Sharif University of Technology, 11155-9567 Tehran, Iran
[b] Dipartimento di Meccanica Strutturale, Università degli Studi di Pavia, Italy
[c] Center for Advanced Numerical Simulation (CeSNA), IUSS, Pavia, Italy
[d] European Centre for Training and Research in Earthquake Engineering (EUCENTRE), Pavia, Italy
[e] Institute for Nano-Science and Technology, Sharif University of Technology, 11155-9567 Tehran, Iran

ARTICLE INFO

Article history:
Received 21 June 2009
Received in final revised form 1 December 2009
Available online 4 January 2010

Keywords:
Shape memory alloys
Non-proportional loading
Phase transformation
Reorientation
Internal variables

ABSTRACT

This paper presents a new phenomenological constitutive model for shape memory alloys, developed within the framework of irreversible thermodynamics and based on a scalar and a tensorial internal variable. In particular, the model uses a measure of the amount of stress-induced martensite as scalar internal variable and the preferred direction of variants as independent tensorial internal variable. Using this approach, it is possible to account for variant reorientation and for the effects of multiaxial non-proportional loadings in a more accurate form than previously done. In particular, we propose a model that has the property of completely decoupling the pure reorientation mechanism from the pure transformation mechanism. Numerical tests show the ability to reproduce main features of shape memory alloys in proportional loadings and also to improve prediction capabilities under non-proportional loadings, as proven by the comparison with several experimental results available in the literature.

1. Introduction

Intelligent, smart or functional materials exhibit special properties that make them a suitable choice for industrial applications in many branches of engineering. Among different types of smart materials, shape memory alloys (SMAs) have unique features known as pseudo-elasticity, one-way and two-way shape memory effects (Duerig et al., 1990; Otsuka and Wayman, 1998). The interest in the mechanical behavior of SMAs is rapidly growing with the increasing number of potential industrial applications. Early commercialization activities, fueled by applications such as rivets, heat engines, couplings, circuit breakers and automobile actuators, started in the 1970s, were intense and often highly secretive (Van Humbeeck, 1999). However, from thereon, the knowledge of SMAs has progressively spread out more and more, up to the fact that nowadays pseudo-elastic Nitinol is a common and well-known engineering material in the medical industry (Duerig et al., 1999; Kuribayashi et al., 2006).

The origin of SMA material features is a reversible thermo-elastic martensitic phase transformation between a high symmetry, austenitic phase and a low symmetry, martensitic phase. Austenite is a solid phase, usually characterized by a body-centered cubic crystallographic structure, which transforms into martensite by means of a lattice shearing mechanism.

* Corresponding author. Address: Department of Mechanical Engineering, Sharif University of Technology, 11155-9567 Tehran, Iran. Tel.: +98 21 6616 5546; fax: +98 21 6600 0021.
E-mail address: naghdabd@sharif.edu (R. Naghdabadi).
[1] Currently visiting Ph.D. student, Dipartimento di Meccanica Strutturale, Università degli Studi di Pavia, Italy.

0749-6419/$ - see front matter © 2009 Elsevier Ltd. All rights reserved.
doi:10.1016/j.ijplas.2009.12.003

When the transformation is driven by a temperature lowering, martensite variants compensate each other, resulting in no macroscopic deformation. However, when the transformation is driven by the application of a load, specific martensite variants favorable to the applied stress direction are preferentially formed, exhibiting a macroscopic shape change in the direction of the applied stress. Upon unloading or heating, this shape change disappears through the reversible conversion of the martensite variants into the parent phase (Funakubo, 1987; Otsuka and Wayman, 1998).

Several experimental studies show that the so-called variant reorientation can be assumed as the main phenomenon in non-proportional loadings of SMAs (Lim and McDowell, 1999; Sittner et al., 1995; Helm, 2001; Helm and Haupt, 2002; Bouvet et al., 2002; Grabe and Bruhns, 2009). Sittner et al. (1995) have studied the tension–torsion behavior of CuAlZnMn shape memory alloys, under box- and triangle-shaped stress and strain control paths. Lim and McDowell (1999) have presented experimental data on a polycrystalline NiTi response to a circular axial-shear strain path. Helm (2001) and Helm and Haupt (2002) have presented extensive biaxial tests on box- and butterfly-shaped strain controlled experiments, while Bouvet et al. (2002) have investigated internal pressure and bi-compression tests on CuAlBe shape memory alloys. Recently, Grabe and Bruhns (2009) have conducted several multiaxial experiments on a polycrystalline NiTi sample within a wide temperature range which show the strong non-linear material response as well as the response path dependencies, highlighting the presence of reorientation processes for complex loading paths.

Considering the experimental observations presented in the cited literature and the fact that several SMA applications undergo non-proportional loadings, it is clear the importance of an effective SMA modeling under arbitrary thermo-mechanical loading conditions, especially for non-proportional situations. Up to now, there have been several attempts to properly reproduce SMA material features in a predictive modeling frame. The resulting models can be in general categorized as either micro, micro–macro or macro. Description of micro-scale features, such as nucleation, interface motion, twin growth, etc., is the main focus of micro models (see among others Ball and James (1987), Abeyaratne and Knowles (1990), Levitas and Stein (1997), Bhattacharya (2003), Idesman et al. (2005), Levitas and Ozsoy (2009a,b)). They are very useful to understand the fundamental phenomenon, although they are not easily applicable at the structural scale. On the other hand, micro–macro studies combine micromechanics and macroscopic thermodynamics to derive constitutive laws of the material (Fischer and Tanaka, 1992; Sun and Hwang, 1993a,b; Lexcellent et al., 1996; Huang and Brinson, 1998; Govindjee and Miehe, 2001; Thamburaja and Anand, 2002; Thamburaja, 2005; Patoor et al., 2006; Pan et al., 2007; Peng et al., 2008; Thamburaja et al., 2009). The predictions by these approaches are successful, but the corresponding time-consuming computations make them inappropriate for engineering applications. Finally, phenomenological or macro approaches use the principles of continuum thermodynamics with internal variables to describe the material behavior and, in general, once cast within numerical methods such as the Finite Element Method (FEM), they are suitable for the analysis of SMA-based devices (Leclercq and Lexcellent, 1996; Auricchio and Sacco, 1997; Auricchio and Taylor, 1997; Auricchio et al., 1997; Bekker and Brinson, 1997; Raniecki and Lexcellent, 1998; Souza et al., 1998; Brocca et al., 2002; Helm and Haupt, 2003; Auricchio et al., 2003; Bouvet et al., 2004; Lagoudas and Entchev, 2004; Muller and Bruhns, 2006; Auricchio et al., 2007; Panico and Brinson, 2007; Popov and Lagoudas, 2007; Thiebaud et al., 2007; Reese and Christ, 2008; Moumni et al., 2008; Christ and Reese, 2009).

In the following, we focus on a phenomenological macro-modeling approach. Selecting an appropriate set of internal variables as macroscopic consequences of the micro-structural changes is the first fundamental issue of phenomenological modeling (Haupt, 2002). In fact, introduction and definition of such internal variables would play a crucial role in arriving at a physically sound constitutive formulation with a simple and consistent structure. Since internal variables are related to micro-structural mechanisms, the definition of their evolution equations is the second fundamental issue of phenomenological modeling and they should be well established with relevant physical considerations (Xiao et al., 2006).

Focusing on shape memory alloys, since the martensitic phase transformation is the basic micro-structural property, in order to incorporate the growth, orientation and reorientation of variants, an appropriate set of internal variables should be able to represent at least a scalar and a directional information (Luig and Bruhns, 2008). So, on one hand, a set of scalar variables is not adequate for a simple description of the material behavior due to the loss of explicit directional information, while, on the other hand, models that have used tensorial internal variables seem to be more successful since they explicitly include simple directional information. In most of the previously proposed models, inelastic strain has been considered as a unique internal variable; following these approaches, in general, the norm of the inelastic strain represents the scalar martensite amount and its direction represents the preferred direction of the variants. Accordingly, in this class of models scalar and directional informations are tightly interconnected, possibly leading to a somehow more limited or constrained modeling approach.

To give more freedom, in the present work a different set of internal variables is proposed with an emphasis on reorientation. A measure of the amount of stress-induced martensite is chosen as a scalar internal variable, being related to the amount of inelastic strain due to stress-induced phase transformation, while the average direction of different variants (or preferred direction of variants) is chosen as a tensorial internal variable, representing the inelastic strain direction. So, using a standard literature terminology (Panico and Brinson, 2007; Bouvet et al., 2004) the internal variables may be clearly interpreted as phase transformation and variant reorientation; in this way, transformation and reorientation can be hopefully described with more flexibility. To the knowledge of the authors, besides the nowadays dated contribution of Auricchio's Ph.D. dissertation (Auricchio, 1995, pp. 69–74), recently there has been only one paper in the literature (Luig and Bruhns, 2008), which starts from similar considerations, following however right away a line of thinking very different from the one proposed here.

The present paper is organized as follows. After a formal definition of the adopted internal variables, Section 2 is devoted to define the Helmholtz free energy function and derive the evolution equations satisfying the Clausius-Duhem inequality. Section 3 presents the model equations in the time-discrete frame. Section 4 is devoted to numerical tests both for proportional and non-proportional loading conditions. In particular, the model ability to properly behave under experimentally investigated loading conditions is tested, presenting also a significant attempt in comparing the model predictions with experimental data available in the literature. Conclusions and summary are finally given in Section 5.

2. A 3-D phenomenological model for SMAs

From a physical point of view, the application of a thermo-mechanical load activates the phase transformation and the preferred martensite variants start to nucleate or shrink (Otsuka and Wayman, 1998). Changing the load direction, another set of variants, that are in the new preferred direction with respect to the applied stress, starts to nucleate and previous variants may grow or shrink depending on the available stress for that direction (this phenomenon is known in the literature as simultaneous forward and reverse transformation under non-proportional loading, see, e.g., Bouvet et al. (2004) and Lim and McDowell (1999)). In the phenomenological framework, we consider the average behavior of variants as the behavior of an equivalent single variant. So when the load direction changes, this equivalent single variant rotates to a new preferred direction.

Accordingly, assuming small strains, we consider the additive strain decomposition:

$$\boldsymbol{\varepsilon} = \boldsymbol{\varepsilon}^{e} + \boldsymbol{\varepsilon}^{ie} \tag{1}$$

where $\boldsymbol{\varepsilon}, \boldsymbol{\varepsilon}^{e}$ and $\boldsymbol{\varepsilon}^{ie}$ are the total, thermo-elastic and inelastic strain, respectively.

In general the inelastic strain $\boldsymbol{\varepsilon}^{ie}$ should include the description of several physical phenomena, ranging, for example, from permanent plasticity and phase transformation up to void generation and fracture. However, in the following we neglect all inelastic phenomena except reversible martensitic phase transformations which are then the only physics to be described by $\boldsymbol{\varepsilon}^{ie}$.

Moreover, keeping in mind all the preliminary shape memory alloy material descriptions addressed in Section 1, in the following we assume to use $\boldsymbol{\varepsilon}^{ie}$ as the only internal variable in the model. However, we do not treat $\boldsymbol{\varepsilon}^{ie}$ as a unique second-order tensor variable, but we clearly distinguish between its norm and direction with the aim of getting more freedom in the modeling. Besides this distinction, the position of non-introducing other micro-structures describing variables leads to obtain a model which is able only to give a very simplified representation of the phenomena occurring at the material micro-mechanical level. In particular there is no attempt to include in the modeling the description of each single martensite variant as well as to obtain a good representation of phenomena such as the phase transformation between single variants.

Accordingly, the choice of dealing with only one second-order tensor internal variable (even decomposed, as mentioned, into its norm and direction) allows only to distinguish between a generic (parent) phase to which no macroscopic strain is associated and a generic (product) phase to which a homogenized macroscopic strain can be associated. This perspective is similar to other effective modeling approaches as the one proposed in Souza et al. (1998), Auricchio and Petrini (2004a), and Auricchio et al. (2007).

According to our previous discussion we now introduce a scalar internal variable q and a tensorial internal variable $\boldsymbol{N}$ such that:

$$\boldsymbol{\varepsilon}^{ie} = q\boldsymbol{N} \tag{2}$$

with

$$\|\boldsymbol{N}\| = 1 \tag{3}$$

where $\|\cdot\|$ is the usual Euclidean norm. According to (2) and (3), it is clear that, supposing $q \geqslant 0$, we have

$$\|\boldsymbol{\varepsilon}^{ie}\| = q \tag{4}$$

Hence, introducing the material parameter ε_L corresponding to the maximum transformation strain reached at the end of the transformation during a uniaxial test, we require

$$0 \leqslant q \leqslant \varepsilon_L \tag{5}$$

Taking time derivative of Eq. (2), we obtain:

$$\dot{\boldsymbol{\varepsilon}}^{ie} = \dot{q}\boldsymbol{N} + q\dot{\boldsymbol{N}} \tag{6}$$

which somehow naturally induces to introduce the following positions:

$$\dot{\boldsymbol{\varepsilon}}^{tr} = \dot{q}\boldsymbol{N} \tag{7}$$

$$\dot{\boldsymbol{\varepsilon}}^{re} = q\dot{\boldsymbol{N}} \tag{8}$$

and using another classical terminology available in the literature, we can interpret Eqs. (7) and (8) as pure transformation and pure reorientation rates, respectively. Accordingly, we can read Eq. (6) as an additive decomposition of the inelastic strain rate as:

$$\dot{\boldsymbol{\varepsilon}}^{ie} = \dot{\boldsymbol{\varepsilon}}^{tr} + \dot{\boldsymbol{\varepsilon}}^{re} \tag{9}$$

Relation (9) is interesting since it states that the inelastic strain evolution induced by the reversible martensite phase transformation is due to two contributions, one from pure transformation and another one from pure reorientation. We also notice that relation (9) is the same as assumed in Panico and Brinson (2007). Moreover, following (9), pure transformation has no effect on the preferred (or average) direction of martensite variants and pure reorientation affects only the direction of variants without directly affecting the amount of martensite. Clearly, also if uncoupled in terms of evolution with respect to their contribution to inelastic strain, the two processes could be related and interconnected through a proper choice of limit functions, as discussed in Section 2.3.

2.1. Helmholtz free energy function

The model assumes the total strain $\boldsymbol{\varepsilon}$ and the absolute temperature T as control variables, the amount of martensite q and the average direction of martensite variants $\boldsymbol{N}$ as internal variables. Introducing the standard strain decomposition into volumetric and deviatoric parts:

$$\boldsymbol{\varepsilon} = \frac{\theta}{3}\,\mathbf{1} + \boldsymbol{e} \tag{10}$$

where $\boldsymbol{e}$ is the deviatoric part of $\boldsymbol{\varepsilon}$, $\theta = \mathrm{tr}(\boldsymbol{\varepsilon})$, while $\mathbf{1}$ is the second-order identity tensor, and assuming $\boldsymbol{\varepsilon}^{ie}$ to be traceless, the free energy density function Ψ for a polycrystalline SMA material is then expressed as the convex potential (see Auricchio and Petrini (2004a) and Souza et al. (1998))

$$\begin{aligned}\Psi(\theta, \boldsymbol{e}, T, q, \boldsymbol{N}, \lambda) = {} & \frac{1}{2}K\theta^2 - 3\alpha K\theta(T - T_r) + G\|\boldsymbol{e} - q\boldsymbol{N}\|^2 + \tau_M(T)q + \frac{1}{2}hq^2 + (u_0 - T\eta_0) + c[(T - T_r) - T\ln(T/T_r)] \\ & + \mathscr{I}_{0,\varepsilon_L}(q) + \lambda(\|\boldsymbol{N}\| - 1)\end{aligned} \tag{11}$$

where K and G are, respectively, the bulk and the shear modulus, $\tau_M(T)$ is a proper function of temperature, h defines the phase transformation hardening, α and c are the thermal expansion coefficient and the heat capacity, while u_0 and η_0 are internal energy and entropy at reference temperature T_r, respectively. We assume $\tau_M(T)$ in the form $\tau_M(T) = \beta\langle T - T_0\rangle$ where β is a material parameter, T_0 another reference temperature and $\langle\cdot\rangle$ the positive part function, defined as:

$$\langle a\rangle = \begin{cases} a & \text{if } a > 0 \\ 0 & \text{otherwise} \end{cases} \tag{12}$$

Moreover, in Eq. (11) we also use the indicator function $\mathscr{I}_{0,\varepsilon_L}$ defined as

$$\mathscr{I}_{0,\varepsilon_L}(q) = \begin{cases} 0 & \text{if } 0 \leqslant q \leqslant \varepsilon_L \\ +\infty & \text{otherwise} \end{cases} \tag{13}$$

in order to enforce inequality constraint (5), while the Lagrange multiplier λ is the constraint force to enforce equality constraint (3).

We remark that we do not consider a fully thermo-mechanical coupled model. Also, the present model as well as some models in the literature (see e.g., Souza et al. (1998), Helm and Haupt (2003), Auricchio and Petrini (2004a), Bouvet et al. (2004), Panico and Brinson (2007), Reese and Christ (2008), Christ and Reese (2009)) does not describe the difference existing between the austenite and the martensite elastic properties (see e.g., Auricchio et al. (2009) for considering different elastic properties).

Starting from the adopted free energy density function Ψ presented in Eq. (11) and following standard arguments, we can derive the constitutive equations

$$\begin{cases} p = \frac{\partial\Psi}{\partial\theta} = K(\theta - 3\alpha(T - T_r)) \\ \boldsymbol{s} = \frac{\partial\Psi}{\partial\boldsymbol{e}} = 2G(\boldsymbol{e} - q\boldsymbol{N}) \\ \eta = -\frac{\partial\Psi}{\partial T} = \eta_0 + 3\alpha K\theta - q\frac{\tau_M(T)}{|T - T_0|} + c\ln(T/T_r) \\ Q = -\frac{\partial\Psi}{\partial q} = \boldsymbol{s} : \boldsymbol{N} - (\tau_M(T) + hq + \gamma) \\ \boldsymbol{X} = -\frac{\partial\Psi}{\partial\boldsymbol{N}} = q\boldsymbol{s} - \lambda\boldsymbol{N} \\ \overline{K} = -\frac{\partial\Psi}{\partial\lambda} = -\|\boldsymbol{N}\| + 1 = 0 \end{cases} \tag{14}$$

where

$$\begin{cases} p = \mathrm{tr}(\boldsymbol{\sigma})/3 \\ \boldsymbol{s} = \boldsymbol{\sigma} - p\mathbf{1} \end{cases} \tag{15}$$

The quantities $\boldsymbol{\sigma}, p, \boldsymbol{s}, \eta$ are, respectively, the Cauchy stress tensor, the volumetric or hydrostatic pressure, the deviatoric part of the stress and the entropy. The thermodynamic forces Q and $\boldsymbol{X}$ are associated to the internal variables q and $\boldsymbol{N}$, while $\overline{K}$ is

the thermodynamic force associated to λ. The variable γ results from the indicator function subdifferential $\partial \mathscr{I}_{0,\varepsilon_L}(q)$ and it is defined as

$$\gamma = \partial \mathscr{I}_{0,\varepsilon_L}(q) = \begin{cases} \gamma_1 \leqslant 0 & \text{if } q = 0 \\ 0 & \text{if } 0 < q < \varepsilon_L \\ \gamma_2 \geqslant 0 & \text{if } q = \varepsilon_L \end{cases} \tag{16}$$

2.2. Evolution equations for the internal variables

According to (14), the mechanical dissipation inequality reduces to

$$D^{mech} = \boldsymbol{\sigma} : \dot{\boldsymbol{\varepsilon}} - (\dot{\Psi} + \eta \dot{T}) = Q\dot{q} + \boldsymbol{X} : \dot{\boldsymbol{N}} \geqslant 0 \tag{17}$$

To satisfy the second law of thermodynamics or the mechanical dissipation inequality (17), we choose the following flow rules for the internal variables:

$$\begin{cases} \dot{q} = \dot{\zeta} Q = \dot{\zeta}(\boldsymbol{s} : \boldsymbol{N} - \tau_M(T) - hq - \gamma) \\ \dot{\boldsymbol{N}} = \dot{\mu} \boldsymbol{X} = \dot{\mu}(q\boldsymbol{s} - \lambda \boldsymbol{N}) \end{cases} \tag{18}$$

where $\dot{\zeta}$ and $\dot{\mu}$ are non-negative consistency parameters.

Moreover, double contracting both sides of Eq. $(18)_2$ with $\boldsymbol{N}$, applying constraint (3) and noting that $\boldsymbol{N} : \dot{\boldsymbol{N}} = 0$ (from time differentiation of $\|\boldsymbol{N}\| = 1$), allow to compute the Lagrange multiplier λ as:

$$\lambda = q\boldsymbol{s} : \boldsymbol{N} \tag{19}$$

Substituting expression (19) for the Lagrange multiplier in the definition $(14)_5$ for the thermodynamic force $\boldsymbol{X}$, we obtain:

$$\boldsymbol{X} = q(\boldsymbol{s} - (\boldsymbol{s} : \boldsymbol{N})\boldsymbol{N}) = q(\mathbb{I} - \boldsymbol{N} \otimes \boldsymbol{N})\boldsymbol{s} = q\boldsymbol{Y} \tag{20}$$

where $\mathbb{I}$ is the fourth-order identity tensor and $\boldsymbol{Y} = (\mathbb{I} - \boldsymbol{N} \otimes \boldsymbol{N})\boldsymbol{s}$ is the stress component normal to $\boldsymbol{N}$. Substituting (20) into (17), the dissipation inequality can be now rewritten as

$$D^{mech} = Q\dot{q} + \boldsymbol{Y} : (q\dot{\boldsymbol{N}}) \geqslant 0 \tag{21}$$

so, the evolution equations can be revised as:

$$\begin{cases} \dot{q} = \dot{\zeta} Q \\ q\dot{\boldsymbol{N}} = \dot{\mu} \boldsymbol{Y} \end{cases} \tag{22}$$

Evolution Eqs. (18) and (22) differ since in (18) $q\boldsymbol{Y}$ is the thermodynamic force of $\dot{\boldsymbol{N}}$, while in (22) $\boldsymbol{Y}$ represents the thermodynamic force for $q\dot{\boldsymbol{N}}$ (i.e., for the reorientation strain rate). Although definitions (18) and (22) are equivalent from a mathematical point of view (since they both satisfy the dissipation inequality), we prefer the latter from a physical point of view.

According to (22), the mechanical dissipation inequality (21) reduces to:

$$D^{mech} = \dot{\zeta} Q^2 + \dot{\mu} \boldsymbol{Y} : \boldsymbol{Y} \geqslant 0 \tag{23}$$

2.3. Limit functions

To describe phase transformation and reorientation evolutions, we choose two limit functions F^{tr} and F^{re} defined as[2]:

$$\begin{cases} F^{tr}(q, Q, \boldsymbol{Y}) = \sqrt{Q^2 + \|\boldsymbol{Y}\|^2} - R^{tr}(q) \\ F^{re}(q, \boldsymbol{Y}) = \|\boldsymbol{Y}\| - R^{re}(q) \end{cases} \tag{24}$$

The model is finally completed by the classical Kuhn–Tucker and consistency conditions, respectively, as follows:

$$\begin{cases} \dot{\zeta} \geqslant 0, \quad F^{tr} \leqslant 0, \quad \dot{\zeta} F^{tr} = 0 \\ \dot{\mu} \geqslant 0, \quad F^{re} \leqslant 0, \quad \dot{\mu} F^{re} = 0 \end{cases} \tag{25}$$

$$\begin{cases} \dot{\zeta} \geqslant 0, \quad \dot{F}^{tr} \leqslant 0, \quad \dot{\zeta} \dot{F}^{tr} = 0 \quad \text{if } F^{tr} = 0 \\ \dot{\mu} \geqslant 0, \quad \dot{F}^{re} \leqslant 0, \quad \dot{\mu} \dot{F}^{re} = 0 \quad \text{if } F^{re} = 0 \end{cases} \tag{26}$$

which also guarantee the positiveness of the energy dissipation (23).

[2] The transformation limit function F^{tr} has the same form as previously proposed in the literature (e.g. see Auricchio and Petrini (2004a) and Souza et al. (1998)). In fact, it can be easily shown that $F^{tr} = \sqrt{Q^2 + \|\boldsymbol{Y}\|^2} = \|\boldsymbol{s} - (\tau_M(T) + hq + \gamma)\boldsymbol{N}\|$.

We remark that, $R^{tr}(q)$ represents the radius of the elastic domain to activate pure transformation while $R^{re}(q)$ represents a threshold value for the component of stress in the direction normal to the preferred direction of variants to activate the variant reorientation. For simplicity in the following we assume R^{tr} and R^{re} constant material parameters instead of functions of q.

We stress that, in order to reproduce the asymmetric behavior in tension and compression shown by SMAs in many experiments, different choices for limit functions should be introduced (see, e.g., Auricchio and Petrini (2004a) and Auricchio et al. (2009) among others). However, this issue is beyond the purpose of the present paper and such an enhancement will be considered in future works.

2.4. Time-continuous constitutive equations review

We now summarize the material law in the time-continuous frame as follows:

$$\begin{cases} p = K(\theta - 3\alpha(T - T_r)) \\ \boldsymbol{s} = 2G(\boldsymbol{e} - q\boldsymbol{N}) \\ Q = \boldsymbol{s} : \boldsymbol{N} - (\tau_M(T) + hq + \gamma) \\ \boldsymbol{Y} = \boldsymbol{s} - (\boldsymbol{s} : \boldsymbol{N})\boldsymbol{N} \\ \dot{q} = \dot{\zeta} Q \\ q\dot{\boldsymbol{N}} = \dot{\mu}\boldsymbol{Y} \\ F^{tr} = \sqrt{Q^2 + \|\boldsymbol{Y}\|^2} - R^{tr} \\ F^{re} = \|\boldsymbol{Y}\| - R^{re} \\ \dot{\zeta} \geqslant 0, F^{tr} \leqslant 0, \dot{\zeta} F^{tr} = 0 \\ \dot{\mu} \geqslant 0, F^{re} \leqslant 0, \dot{\mu} F^{re} = 0 \end{cases} \tag{27}$$

Adopting a slightly different notation, Appendix A proposes an equivalent form of Eq. (27) which is more consistent with different papers in the literature, such as Souza et al. (1998), Auricchio and Petrini (2002), and Panico and Brinson (2007).

We may observe that, in the case of proportional loading, by definition $\boldsymbol{N} = \boldsymbol{s}/\|\boldsymbol{s}\|$, hence $\boldsymbol{Y} = \boldsymbol{0}$ and $\dot{\mu} = 0$; so the proposed model reduces to:

$$\begin{cases} Q = \|\boldsymbol{s}\| - (\tau_M(T) + hq + \gamma) \\ \dot{q} = \dot{\zeta} Q \\ F^{tr} = |Q| - R^{tr} \end{cases} \tag{28}$$

Accordingly, for a proportional loading, the preferred variant direction coincides with the deviatoric stress direction and the only unknown, i.e., the martensite amount q, can be computed by (28).

Now, comparing Eqs. $(27)_7$ and $(28)_3$ we can also get some insights on how non-proportional loadings affect the model response. In fact, according to $(28)_3$, the hysteresis size in a proportional loading is constant and is equal to R^{tr}, while loading non-proportionality reduces the hysteresis size, as given by $(27)_7$, of an amount directly related to $\|\boldsymbol{Y}\|$, up to a maximum value of R^{re}; this change in the hysteresis size can be interpreted as the reorientation effect on the transformation. On the other hand, due to the simple limit function adopted for reorientation and based on assuming a constant threshold value for $\|\boldsymbol{Y}\|$ to activate reorientation, we conclude that pure transformation does not affect reorientation.

3. Time-discrete frame

As the aim of this paper is to show the constitutive model behavior without focusing on algorithmic problems, a backward-Euler integration algorithm with small time steps is used for the solution of the examples in Section 4, and the solution to the non-linear system is found by means of the function *fsolve* implemented in the Optimization Toolbox of the program *MATLAB®*.

Assuming to be given the state $(p_n, \boldsymbol{s}_n, q_n, \boldsymbol{N}_n)$ at time t_n, the actual total strain $(\theta, \boldsymbol{e})$ and temperature T at time t_{n+1} (note that for notation simplicity here and in the following we drop the subindex $n+1$ for all of the variables computed at time t_{n+1}), the updated values $(p, \boldsymbol{s}, q, \boldsymbol{N})$ can be computed from the following time-discrete system:

$$\begin{cases} p = K(\theta - 3\alpha(T - T_r)) \\ \boldsymbol{s} = 2G(\boldsymbol{e} - q\boldsymbol{N}) \\ Q = \boldsymbol{s} : \boldsymbol{N} - (\tau_M(T) + hq + \gamma) \\ \boldsymbol{Y} = \boldsymbol{s} - (\boldsymbol{s} : \boldsymbol{N})\boldsymbol{N} \\ q = q_n + \Delta\zeta Q \\ q\boldsymbol{N} = q\boldsymbol{N}_n + \Delta\mu\boldsymbol{Y} \\ F^{tr} = \sqrt{Q^2 + \|\boldsymbol{Y}\|^2} - R^{tr} \\ F^{re} = \|\boldsymbol{Y}\| - R^{re} \end{cases} \tag{29}$$

along with the requirements

$$\begin{cases} \Delta\zeta \geqslant 0, \quad F^{tr} \leqslant 0, \quad \Delta\zeta F^{tr} = 0 \\ \Delta\mu \geqslant 0, \quad F^{re} \leqslant 0, \quad \Delta\mu F^{re} = 0 \end{cases} \tag{30}$$

The solution of the discrete model is performed by means of an elastic-predictor inelastic-corrector return map procedure as in classical plasticity problems (Simo and Hughes, 1998). An elastic trial state is evaluated keeping frozen the internal variables, then trial values of the limit functions are computed to verify the admissibility of the trial state. If this is not the case, the step is inelastic and the evolution equations have to be integrated. Due to decoupling of reorientation from transformation, we first solve for the new direction of variants $\boldsymbol{N}$ by solving $(29)_6$ and $(29)_8$. Then using the new direction, we find the martensite amount q solving $(29)_5$ and $(29)_7$ and distinguishing two inelastic phases: a non-saturated phase $(q < \varepsilon_L, \gamma = 0)$ and a saturated one $(q = \varepsilon_L, \gamma \geqslant 0)$. In the solution procedure we start assuming to be in a non-saturated phase, and when convergence is attained we check if our assumption is violated. If the non-saturated solution is not admissible, we set $q = \varepsilon_L$.

As a closing remark, we wish to point out the definition of $\boldsymbol{N}$ in the case $\boldsymbol{\varepsilon}^{ie} = \boldsymbol{0}$. Since for the case $q = 0$, the inelastic strain vanishes independently from $\boldsymbol{N}$, we define $\boldsymbol{N}$ in a way to guarantee its continuity, i.e. we take $\boldsymbol{N} = \boldsymbol{s}/\|\boldsymbol{s}\|$ when $q = 0$. We stress that in this way there is no need to use regularization as done in previous works (Auricchio and Petrini, 2004a; Panico and Brinson, 2007; Helm and Haupt, 2003).

4. Model predictions for proportional and non-proportional loadings

The present section deals with several uniaxial and multiaxial proportional as well as non-proportional loading conditions. In particular, Section 4.1 presents the results for uniaxial tests at three different temperatures to show the model capability of reproducing basic effects such as pseudo-elasticity and shape memory effect. Section 4.2 presents the results for multiaxial combined tension–torsion proportional tests with two different proportionality factors. Section 4.3 presents the results for several non-proportional loading paths comparing them also with experimental data available in the literature.

For all the simulations discussed in Section 4.1 and in Section 4.2 as well as for the first set of simulations discussed in Section 4.3, we adopt the material parameters reported in Table 1. It is worthful to note that no value is attributed to R^{re} since this parameter is not significant for the case of proportional loadings. Moreover, material parameters reported in Table 1 do not specifically describe any alloy since they are not deduced from experimental data, but simply looking at similar material parameters presented in the literature (Helm and Haupt, 2003; Panico and Brinson, 2007). The chosen material parameters correspond to the following characteristic temperatures $M_f^0 = 306, M_s^0 = 310, A_s^0 = 317$ and $A_f^0 = 319$ (Panico and Brinson, 2007) where M_s^0, M_f^0, A_s^0 and A_f^0 are martensite start, martensite finish, austenite start and austenite finish temperatures at stress-free condition, respectively. For simulation of the non-proportional loading paths in Section 4.3, the material parameters are directly identified from experimental data available in the literature and they are discussed in that section. Finally, in all examples we assume the material to be initially in a generic parent phase $(q = 0)$. Also, since the thermal expansion is a secondary effect compared to martensite production, we set the thermal expansion material coefficient equal to zero in all simulations.

Before starting to present the model performance, we wish to point out that we tried to present as much as possible a wide and complete set of loading situations. Unfortunately, in the literature, there is no corresponding set of experimental data on a unique material (this is the reason for dealing with two sets of material data in Section 4.3 as discussed above), as well as there is no other macro-modeling paper addressing all the extensive sets of loading conditions reported here. Finally connected to the large variety of situations considered, we cannot absolutely claim that the proposed model is adequate and satisfactory in all the tests, but we try to clearly and honestly address model performance in particular in comparison with what is currently available in the literature.

4.1. Uniaxial tests

We start considering uniaxial loading-unloading at the three different constant temperatures of 300, 320 and 340 K and up to a maximum stress value of 600 MPa. As shown in Fig. 1, the model is able to reproduce the characteristic hysteresis

Table 1
Material parameters used in the numerical tests.

Parameter	Value	Unit
E	68,400	MPa
ν	0.36	–
h	369.35	MPa
ε_L	4.65	%
β	8.165	MPa K^{-1}
T_0	310	K
R^{tr}	72.6	MPa
R^{re}	10	MPa

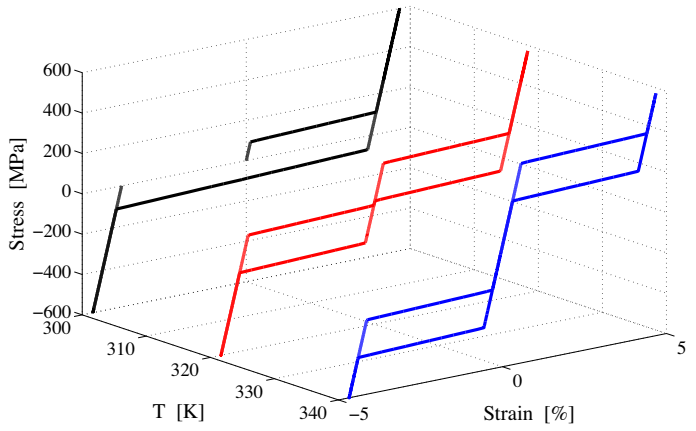

Fig. 1. Model response for tension-compression uniaxial loading at constant temperature.

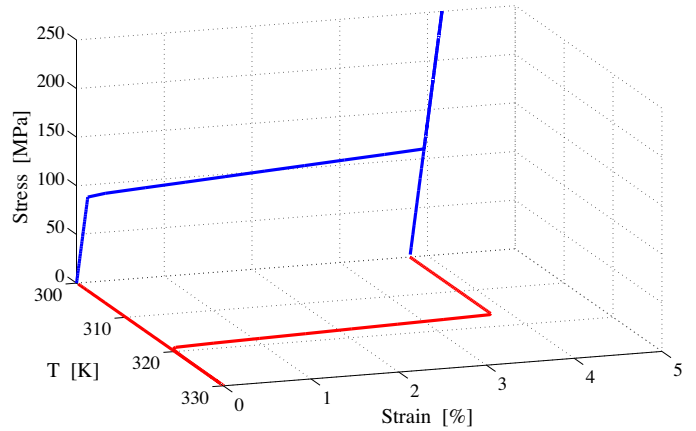

Fig. 2. Model reproduction of the shape memory effect.

loops of SMAs both in tension and compression. Furthermore, critical transformation stress increases with temperature, as experimentally observed. Then, to test the model reproduction of the shape memory effect, we simulate a thermo-mechanical loading (see Fig. 2). At a temperature of 300 K, the material is loaded up to a maximum stress of 250 MPa, so it fully transforms to oriented martensite. Keeping the temperature constant and unloading to zero stress results in a mechanically unrecoverable residual strain, which can be however recovered after heating the material above the austenite finish temperature. Finally, cooling the strain-free material to the initial temperature does not alter its strain or stress state. Sharp increase of stress over the plateau in Figs. 1 and 2 is also predicted by the model as it is only due to elastic behavior of stress-induced martensite phase in the saturated case (fully transformed to martensite) and no phase transformation can occur anymore.

4.2. Multiaxial proportional tests

Following the idea of Sittner et al. (1995) we now investigate the model predictions in the superelastic range under two different proportional loading paths characterized by the same equivalent stress (defined as $\sigma_{eq} = \sqrt{\sigma^2 + 3\tau^2}$), but with different proportionality factors. In particular, we set the temperature equal to 330 K and, as suggested by Sittner et al. (1995), we consider two paths, presented in Fig. 3, such that in path 1 tension is governing, while in path 2 shear is governing. Figs. 4 and 5 show the model response under these loading paths, which qualitatively reproduces experimentally observed material response.

4.3. Multiaxial non-proportional tests

We now start investigating the model predictions for non-proportional loadings, still focusing on the material superelastic range. Accordingly, in all the examples proposed in the following, the test temperature is set to 320 K, for which a superelastic behavior is expected.

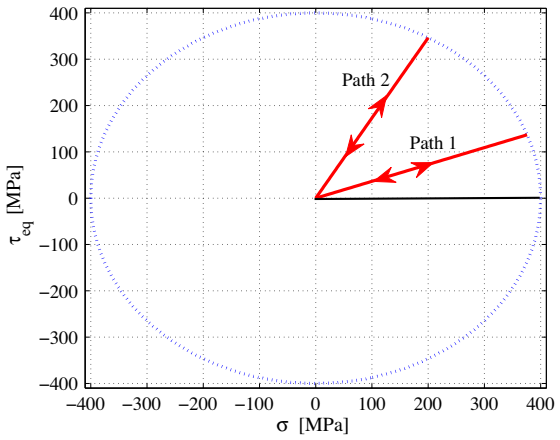

Fig. 3. Stress path in proportional loading $\left(\tau_{eq}=\sqrt{3}\tau,\ \tan(\alpha)=\frac{\sqrt{3}\tau}{\sigma},\alpha=\frac{\pi}{9},\frac{\pi}{3}\right)$.

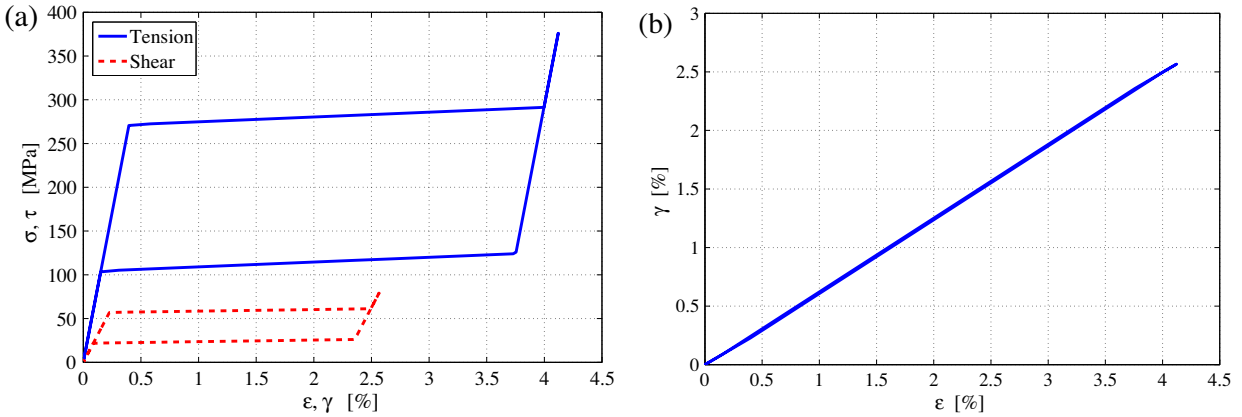

Fig. 4. Model prediction for proportional path 1: (a) stress–strain curves, (b) axial-shear strain response.

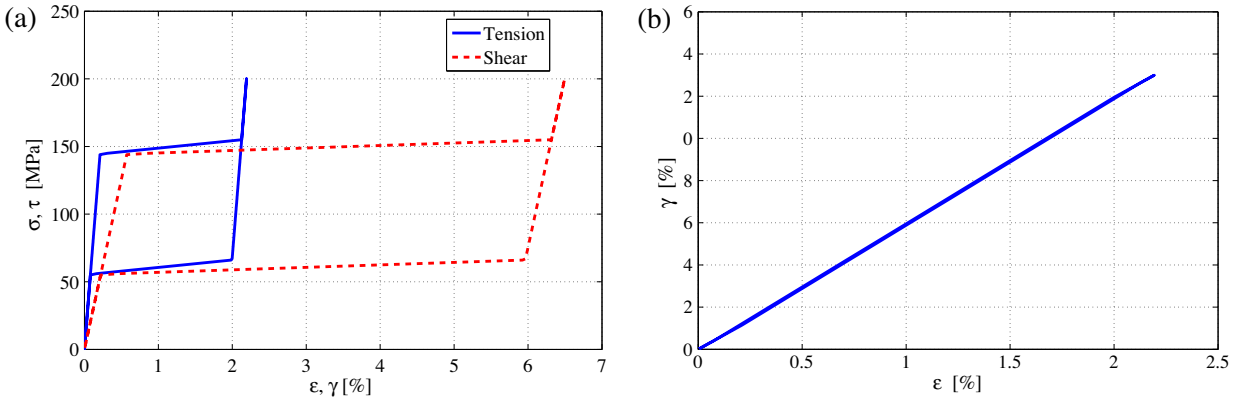

Fig. 5. Model prediction for proportional path 2: (a) stress–strain curves, (b) axial-shear strain response.

Following the recently published experimental study by Grabe and Bruhns (2009) we start considering a tension-shear test, where stresses are varied in the range ±250 MPa following a squared-shaped history, as reported in Fig. 6a. Since during the first tension loading segment, the material fully transforms to oriented martensite, the entire subsequent part of the loading only involves reorientation. A comparison between predictions of the proposed model and the model discussed

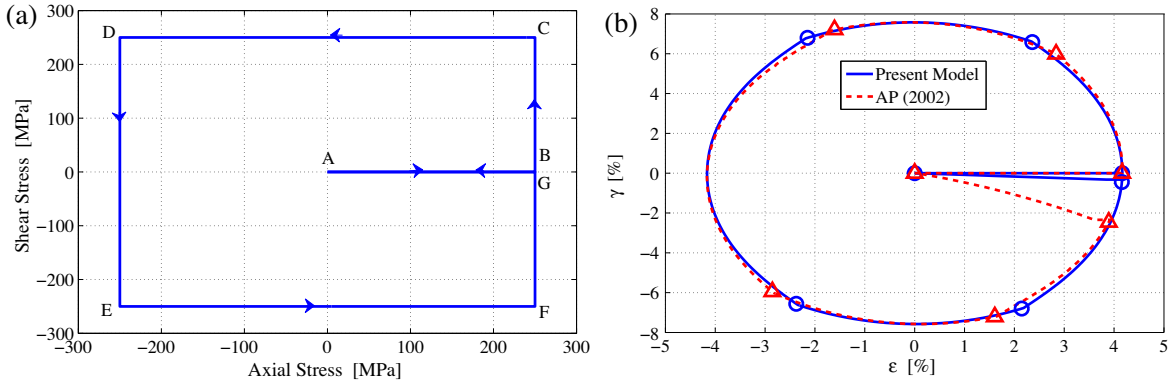

Fig. 6. Biaxial non-proportional loading: (a) axial-shear stress path, (b) comparison of model predictions for axial-shear strain response.

by Auricchio and Petrini (2002) (in the following, we refer to this model as AP (2002)) is presented in Fig. 6b. Circle and triangle symbols in Fig. 6b correspond to points A to G in the stress path for the proposed and for the AP (2002) models, respectively.

It is interesting to observe that in the proposed model, an increase of the value corresponding to the material parameter R^{re} would produce a clockwise rotation of the response path, while there is no equivalent material parameter in AP (2002) to tune the response path rotation. The rotation of the response path has also been observed in the experimental study by Grabe and Bruhns (2009).

Now, we compare the model prediction with experimental data available in the literature. For this purpose we employ the results of tension–torsion experiments with thin wall specimens of CuAlZnMn polycrystalline SMAs reported by Sittner et al. (1995). Since the model discussed in the previous section has been based on an idealized SMA behavior, ignoring asymmetric behavior in tension–compression, subloops, non-constant hysteresis size, etc., only an approximate description of the experimentally observed behavior is possible, and so the comparison between the model prediction and the experimental data will be discussed from a qualitative point of view. We identify material parameters (reported in Table 2) using the experimental data reported by Sittner et al. (1995) for proportional tension and torsion tests (Fig. 7). Fig. 7a and b show the corresponding model predictions.

After material parameter identification, we simulate some of the combined non-proportional loading paths proposed and experimentally realized in Sittner et al. (1995). Fig. 8a shows a biaxial non-proportional stress path. Initially, an axial stress of 240 MPa is applied and then the shear stress is increased up to approximately 195 MPa, while tension is kept constant. During stages 3 and 4, first tension and then shear are sequentially unloaded, respectively.

Fig. 8b, c and d show the comparison between the predictions of the proposed model, of the model presented by Auricchio and Petrini (2002) (referred to as AP (2002)) and the model presented by Panico and Brinson (2007) (referred to as PB (2007)) with the experimental data in terms of shear strain versus normal strain, normal stress versus normal strain and shear stress versus shear strain, respectively. A qualitatively good agreement between experiments and simulations is obtained for the proposed model when $R^{re}=R^{tr}$, which is able to reproduce the main characteristics of the experimentally observed behaviors. This is particularly true for the coupling between axial and shear strains both in stages 2 and 3.

Moreover, the proposed model can predict the crossing in the shear response observed experimentally in Fig. 8d. Although there is a good qualitative agreement between the proposed model and experimental data, some drawbacks are observed, for example in the second stage of loading, where the coupling effect is not completely in agreement with experiments. This can be partially due to the very simple structure of the proposed model, i.e. assuming R^{re} as a constant material parameter. In order to investigate more this drawback, we present the simulation results along with comparison with AP (2002) and experimental data for two other non-proportional loading paths proposed by Sittner et al. (1995). Accordingly, Figs. 9 and 10 present the results for triangle- and L-shaped stress paths, respectively.

Table 2
Material parameters adopted for Sittner et al. (1995) experiment.

Parameter	Value	Unit
E	30,700	MPa
ν	0.35	–
h	11,000	MPa
ε_L	4.9	%
τ_M	150	MPa
T	285	K
R^{tr}	63.3	MPa

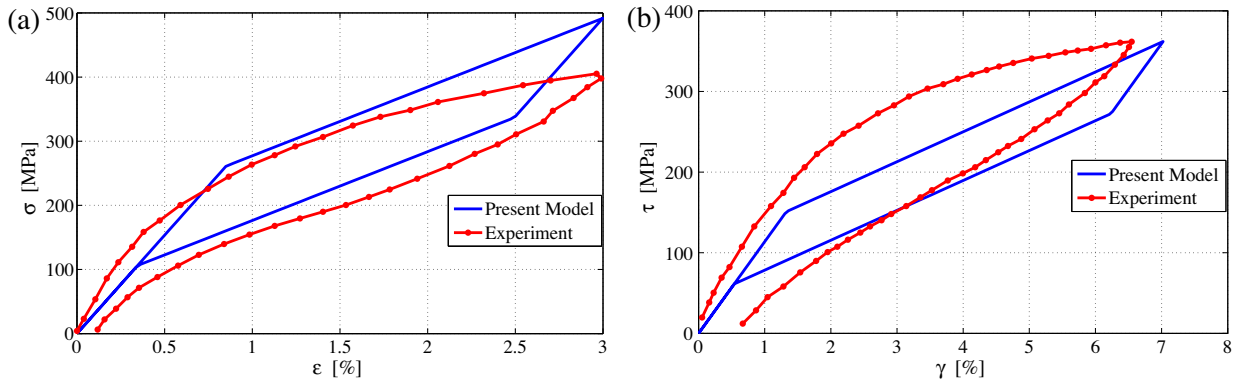

Fig. 7. Model prediction compared to the experimental data by Sittner et al. (1995): (a) uniaxial tension, (b) torsion.

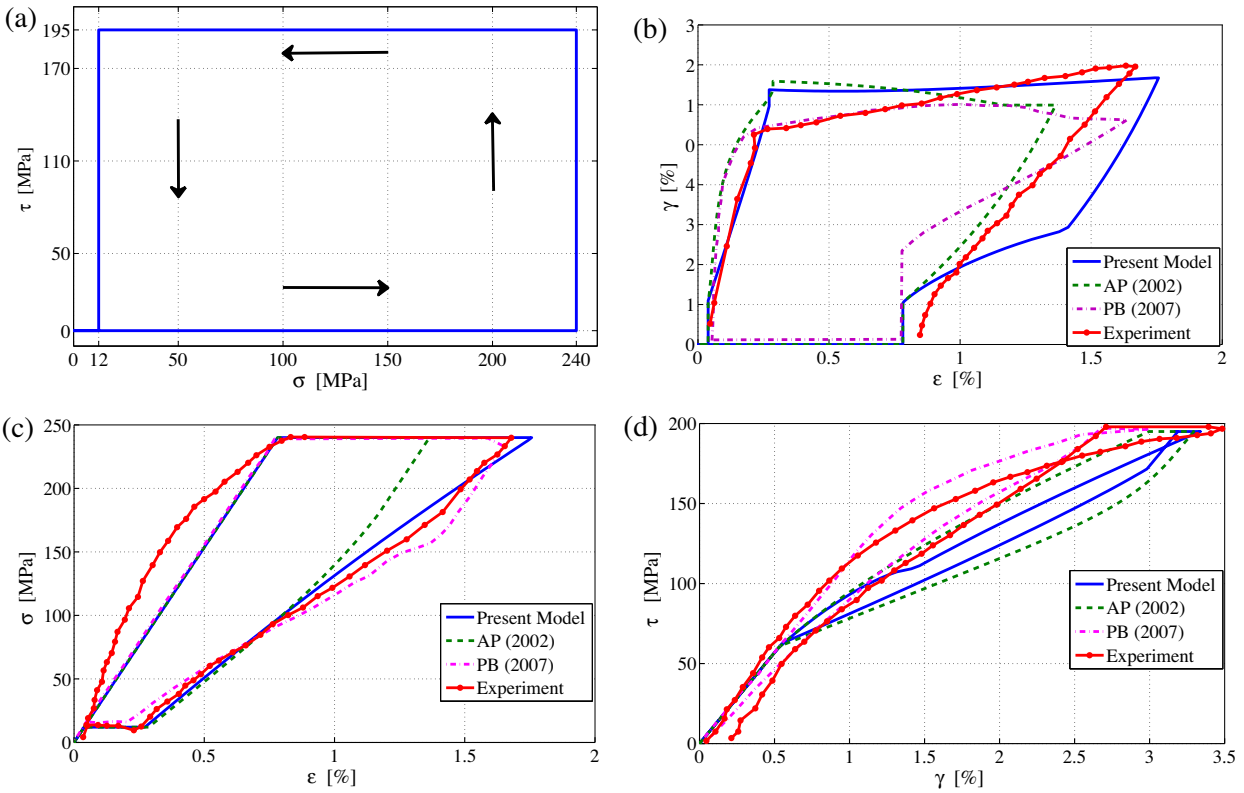

Fig. 8. Comparison between model predictions and experimental data (Sittner et al., 1995): (a) non-proportional biaxial tension-shear path, (b) axial-shear strain response, (c) axial stress–axial strain response, (d) shear stress–shear strain response.

The proposed model captures the basic features of material response to the mentioned loading situations although some differences can be clearly noted if compared to the AP (2002) model. This aspect should be investigated in future studies.

We finally consider the experimental data reported by Bouvet et al. (2002, 2004) on a tubular CuAlBe specimen. In particular, focusing only on experimental tension test data, we choose the material parameters reported in Table 3. Fig. 11 shows a comparison between the proposed model response and experimental data. Using only uniaxial data it is clearly not possible to set a value for the reorientation activation threshold, which is the only parameter left to be determined.

Biaxial tension/compression-internal pressure tests have been performed on tubular CuAlBe specimens to investigate the effects of non-proportionality of the loading path on the superelastic behavior of SMAs (Bouvet et al., 2002). Since we are using an idealized model, tension–tension experimental data are chosen to reduce tension–compression asymmetry effects, although the material elastic behavior is transversely isotropic ($E_r = 84$ GPa, $E_z = 68$ GPa (Bouvet et al., 2002)). So we concentrate only on the qualitative behavior.

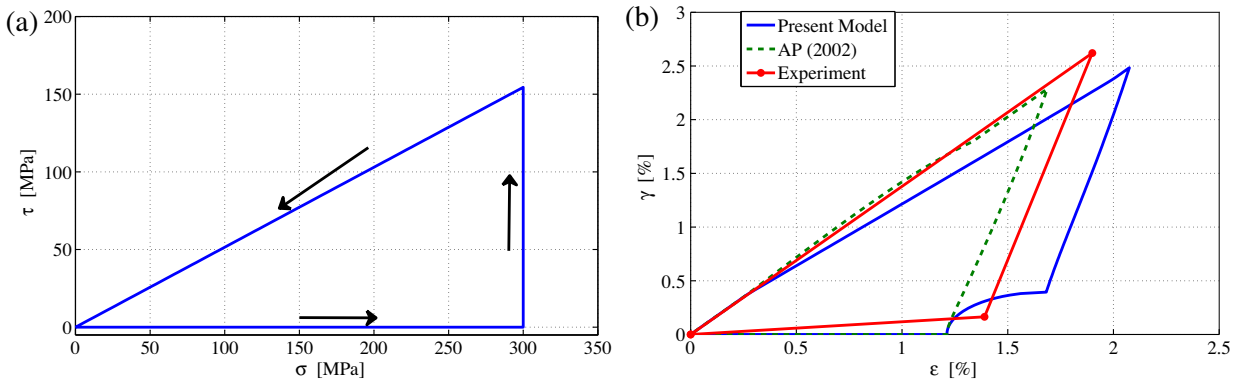

Fig. 9. Proposed model prediction and comparison with AP (2002) and experimental results (Sittner et al., 1995): (a) axial-shear triangle-shaped stress path, (b) axial-shear strain response.

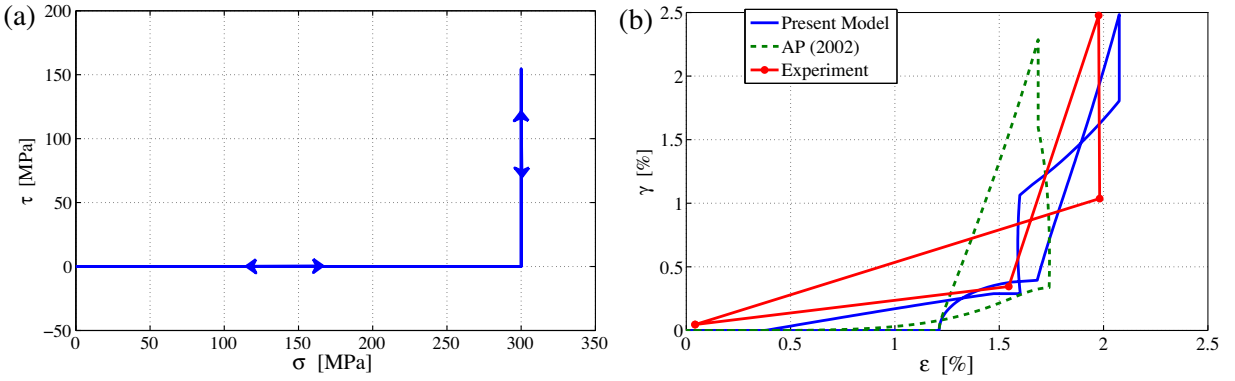

Fig. 10. Proposed model prediction and comparison with AP (2002) and experimental results (Sittner et al., 1995): (a) axial-shear L-shaped stress path, (b) axial-shear strain response.

Table 3
Material parameters adopted for (Bouvet et al., 2002, 2004) experiment.

Parameter	Value	Unit
E	75,000	MPa
v	0.3	–
h	4233	MPa
ε_L	5.85	%
τ_M	51	MPa
T	305	K
R^{tr}	16	MPa

With the selected material parameters, we try to reproduce the material response under a non-proportional biaxial tension-internal pressure loading. Fig. 12a shows a non-proportional biaxial tension test, in which initially a tension stress of 140 MPa in the axial direction is applied, and then an internal pressure is applied to increase the hoop tension stress up to 140 MPa, while the axial tension is kept constant. Then, sequentially, axial tension and internal pressure are removed.

A good correlation between the proposed model predictions and the experimental data is observed for $R^{re} = R^{tr}$. Fig. 12b, c and d present the comparison between the present model prediction, AP (2002) model prediction and experimental results (Bouvet et al., 2002), respectively, in terms of hoop versus axial strain (Fig. 12b), axial stress versus axial strain (Fig. 12c), hoop stress versus hoop strain (Fig. 12d). The model prediction for the axial direction is in good qualitative agreement with the experimental data, but there is a discrepancy with the experiments in the prediction for the hoop direction.

We then consider another set of experimental data, reported in Bouvet et al. (2004), obtained on the same CuAlBe specimen. Fig. 13a shows the loading path, which is identical to the one considered in the previous test (Fig. 12a) but it is now applied in the reverse direction (i.e., in Fig. 13a it is clockwise while in Fig. 12a it is counter-clockwise).

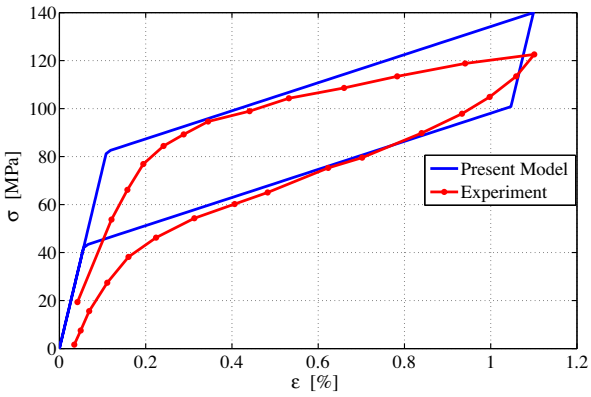

Fig. 11. Uniaxial tension behavior predicted by the model and comparison with experimental results from Bouvet et al. (2004).

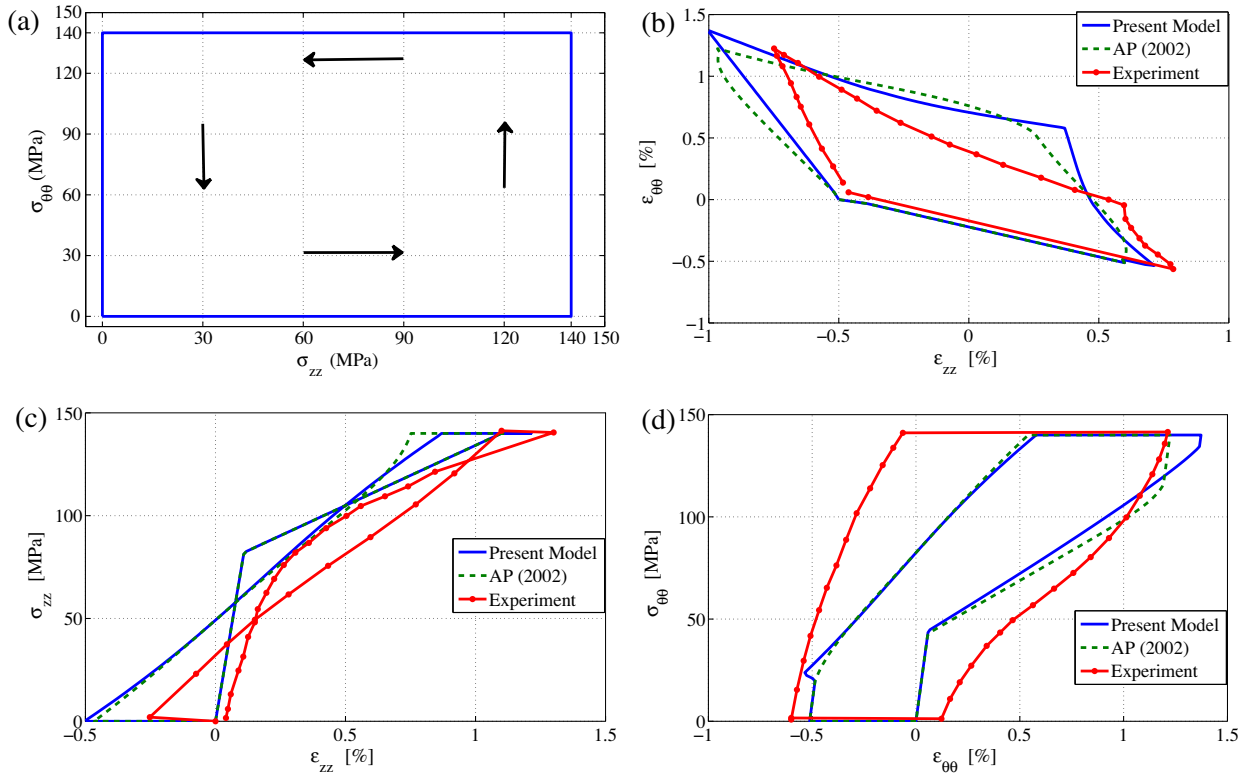

Fig. 12. Comparison between simulation and experimental results (Bouvet et al., 2002): (a) non-proportional biaxial loading path, (b) corresponding strain path, (c) axial stress–strain curve, (d) hoop stress–strain curve.

Fig. 13b, c and d present the comparison between the present model and AP (2002) predictions and experimental results (Bouvet et al., 2004). As a reference we also include the digitized data related to the model proposed in Bouvet et al. (2004) (referred to as BE (2004)), which takes into account the tension–compression asymmetry and the return point memory effects.

A good correlation between the proposed model predictions and the experimental data is again observed for $R^{re} = R^{tr}$. This equality can be interpreted as the macroscopic consequence of microscopic simultaneous forward and reverse transformation, which can link the phase transformation parameter to the reorientation one. We do not limit the model to this case, but this will be the subject of future studies.

According to all the tests reported, we may conclude that the proposed model can describe the reorientation phenomenon in SMAs under non-proportional loading in a good qualitative way, but it needs some improvements, such as considering the material parameter R^{re} as a function of q, which will be the subject of future works.

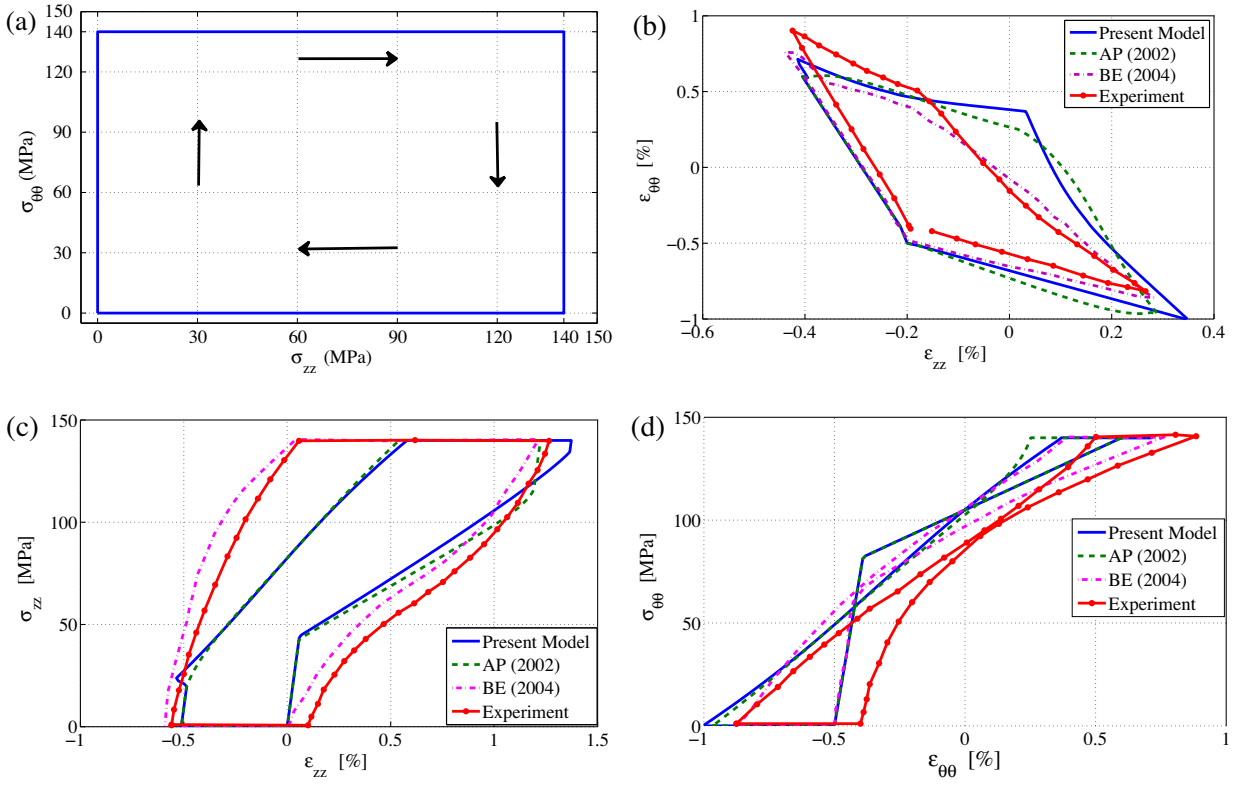

Fig. 13. Comparison between simulation and experimental results (Bouvet et al., 2004): (a) non-proportional biaxial loading path, (b) corresponding strain path, (c) axial stress–strain curve, (d) hoop stress–strain curve.

Since the internal variables are somehow related to micromechanical phenomena, we can find similar concepts if compared with micromechanics-based studies. For example the thermodynamic forces and the dissipation inequality arising from the present model are in correlation with analogous expressions in Levitas and Ozsoy (2009a). Deriving limit functions motivated by micromechanical studies (e.g., Sun and Hwang, 1993a; Levitas and Stein, 1997; Levitas and Ozsoy, 2009a) is an interesting subject for future studies which if adopted, could improve the proposed model capabilities.

5. Conclusions

In this study we present some new features of SMA constitutive modeling under non-proportional loading. Chosen on a physical basis, a new set of internal variables is introduced. Such variables describe in a clear way phase transformation and reorientation. Within the proposed approach, transformation evolves only due to the stress component in the direction of preferred variants while only the component of stress normal to the variant preferred direction affects variant reorientation. Comparison of the proposed model predictions with experimental data under different non-proportional loadings shows a good qualitative agreement which verifies the proposed model capabilities in capturing the reorientation phenomenon.

Acknowledgements

Financial supports from the Iranian Ministry of Science, Research and Technology and also National Elites Foundation to the first author is gratefully acknowledged.

F. Auricchio and A. Reali have been partially supported by the European Science Foundation through the EUROCORES S3T project "SMARTeR: Shape Memory Alloys to Regulate Transient Responses in civil engineering" and by the European Research Council through the Starting Independent Research Grant "BioSMA: Mathematics for Shape Memory Technologies in Biomechanics".

Appendix A. The proposed model in terms of the tensorial internal variable $\boldsymbol{e}^{in}$

To present the proposed model in terms of the internal variable $\boldsymbol{e}^{in}$, we substitute q with $\|\boldsymbol{e}^{in}\|$ and $\boldsymbol{N}$ with $\frac{\boldsymbol{e}^{in}}{\|\boldsymbol{e}^{in}\|}$ in (27) and use relation (6) to find $\dot{\boldsymbol{e}}^{in}$, which results in:

$$\begin{cases} p = K(\theta - 3\alpha(T - T_r)) \\ \boldsymbol{s} = 2G(\boldsymbol{e} - \boldsymbol{e^{in}}) \\ \boldsymbol{R} = \boldsymbol{s} - \boldsymbol{\alpha} \\ \boldsymbol{Y} = \boldsymbol{s} - (\boldsymbol{s} : \boldsymbol{N})\boldsymbol{N} \\ \boldsymbol{\alpha} = (\tau_M(T) + h\|\boldsymbol{e^{in}}\| + \gamma)\frac{\boldsymbol{e^{in}}}{\|\boldsymbol{e^{in}}\|} \\ \dot{\boldsymbol{e}}^{in} = \dot{\zeta}\boldsymbol{R} + (\dot{\mu} - \dot{\zeta})\boldsymbol{Y} \\ F^{tr} = \|\boldsymbol{R}\| - R^{tr} \\ F^{re} = \|\boldsymbol{Y}\| - R^{re} \end{cases} \tag{31}$$

The following classical Kuhn–Tucker conditions complete the model:

$$\begin{cases} \dot{\zeta} \geqslant 0, \quad F^{tr} \leqslant 0, \quad \dot{\zeta}F^{tr} = 0 \\ \dot{\mu} \geqslant 0, \quad F^{re} \leqslant 0, \quad \dot{\mu}F^{re} = 0 \end{cases} \tag{32}$$

For more details see Arghavani (2010).

References

Abeyaratne, R., Knowles, J.K., 1990. On the driving traction acting on a surface of strain discontinuity in a continuum. Journal of the Mechanics and Physics of Solids 38 (3), 345–360.

Arghavani, J., 2010. Thermomechanical behavior of shape memory alloys under nonproportional loading: constitutive modelling and numerical implementation in small and finite strains. Ph.D. thesis, Sharif University of Technology, Iran.

Auricchio, F., 1995. Shape memory alloys – applications, micromechanics, macromodeling and numerical simulations. Ph.D. thesis, University of California at Berkely.

Auricchio, F., Petrini, L., 2002. Improvements and algorithmical considerations on a recent three-dimensional model describing stress-induced solid phase transformations. International Journal for Numerical Methods in Engineering 55 (11), 1255–1284.

Auricchio, F., Petrini, L., 2004a. A three-dimensional model describing stress-temperature induced solid phase transformations: thermomechanical coupling and hybrid composite applications. International Journal for Numerical Methods in Engineering 61 (5), 716–737.

Auricchio, F., Sacco, E., 1997. A one-dimensional model for superelastic shape-memory alloys with different elastic properties between austenite and martensite. International Journal of Non-Linear Mechanics 32 (6), 1101–1114.

Auricchio, F., Taylor, R.L., 1997. Shape-memory alloys: modelling and numerical simulations of the finite-strain superelastic behavior. Computer Methods in Applied Mechanics and Engineering 143 (1–2), 175–194.

Auricchio, F., Taylor, R.L., Lubliner, J., 1997. Shape-memory alloys: macromodelling and numerical simulations of the superelastic behavior. Computer Methods in Applied Mechanics and Engineering 146 (3–4), 281–312.

Auricchio, F., Marfia, S., Sacco, E., 2003. Modelling of SMA materials: training and two way memory effects. Computers and Structures 81 (24–25), 2301–2317.

Auricchio, F., Reali, A., Stefanelli, U., 2007. A three-dimensional model describing stress-induced solid phase transformation with permanent inelasticity. International Journal of Plasticity 23 (2), 207–226.

Auricchio, F., Reali, A., Stefanelli, U., 2009. A macroscopic 1D model for shape memory alloys including asymmetric behaviors and transformation-dependent elastic properties. Computer Methods in Applied Mechanics and Engineering 198 (17–20), 1631–1637.

Ball, J.M., James, R.D., 1987. Fine phase mixtures as minimizers of energy. Archive for Rational Mechanics and Analysis 100, 13–52.

Bekker, A., Brinson, L.C., 1997. Temperature-induced phase transformation in a shape memory alloy: phase diagram based kinetics approach. Journal of the Mechanics and Physics of Solids 45 (6), 949–988.

Bhattacharya, K., 2003. Microstructure of Martensite. Oxford University Press, Oxford.

Bouvet, C., Calloch, S., Lexcellent, C., 2002. Mechanical behavior of a Cu–Al–Be shape memory alloy under multiaxial proportional and nonproportional loadings. Journal of Engineering Materials and Technology 124, 112–124.

Bouvet, C., Calloch, S., Lexcellent, C., 2004. A phenomenological model for pseudoelasticity of shape memory alloys under multiaxial proportional and nonproportional loadings. European Journal of Mechanics A/Solids 23 (1), 37–61.

Brocca, M., Brinson, L.C., Bazant, Z.P., 2002. Three-dimensional constitutive model for shape memory alloys based on microplane model. Journal of the Mechanics and Physics of Solids 50 (5), 1051–1077.

Christ, D., Reese, S., 2009. A finite element model for shape memory alloys considering thermomechanical couplings at large strains. International Journal of Solids and Structures 46 (20), 3694–3709.

Duerig, T.W., Melton, K.N., Stoekel, D., Wayman, C.M., 1990. Engineering Aspects of Shape Memory Alloys. Butterworth-Heinemann, London.

Duerig, T., Pelton, A., Stckel, D., 1999. An overview of nitinol medical applications. Materials Science and Engineering A, 149–160.

Fischer, F., Tanaka, K., 1992. A micromechanical model for the kinetics of martensitic transformation. International Journal of Solids and Structures 29 (14–15), 1723–1728.

Funakubo, H., 1987. Shape Memory Alloys. Gordon and Breach Science Publishers, New York.

Govindjee, S., Miehe, C., 2001. A multi-variant martensitic phase transformation model: formulation and numerical implementation. Computer Methods in Applied Mechanics and Engineering 191 (3–5), 215–238.

Grabe, C., Bruhns, O., 2009. Path dependence and multiaxial behavior of a polycrystalline NiTi alloy within the pseudoelastic and pseudoplastic temperature regimes. International Journal of Plasticity 25, 513–545.

Haupt, P., 2002. Continuum Mechanics and Theory of Materials. Springer Publication House.

Helm, D., 2001. Formgedachtnislegierungen experimentelle untersuchung, phanomenologische modellierung und numerische simulation der thermomechanischen materialeigenschaften. Ph.D. thesis, Universitat Gesamthochschule, Kassel.

Helm, D., Haupt, P., 2002. Thermomechanical representation of the multiaxial behavior of shape memory alloys. In: Lynch, C.S. (Ed.), Proceedings of SPIE Smart Structures and Materials 2002. Active Materials: Behavior and Mechanics, vol. 4699, pp. 343–354.

Helm, D., Haupt, P., 2003. Shape memory behaviour: modelling within continuum thermomechanics. International Journal of Solids and Structures 40 (4), 827–849.

Huang, M., Brinson, L.C., 1998. A multivariant model for single crystal shape memory alloy behavior. Journal of the Mechanics and Physics of Solids 46 (8), 1379–1409.

Idesman, A., Levitas, V., Preston, D., Cho, J.-Y., 2005. Finite element simulations of martensitic phase transitions and microstructures based on a strain softening model. Journal of the Mechanics and Physics of Solids 53 (3), 495–523.

Kuribayashi, K., Tsuchiya, K., You, Z., Tomus, D., Umemoto, M., Ito, T., Sasaki, M., 2006. Self-deployable origami stent grafts as a biomedical application of Ni-rich TiNi shape memory alloy foil. Materials Science and Engineering A 419 (1–2), 131–137.
Lagoudas, D.C., Entchev, P.B., 2004. Modeling of transformation-induced plasticity and its effect on the behavior of porous shape memory alloys. Part I: constitutive model for fully dense SMAs. Mechanics of Materials 36 (9), 865–892.
Leclercq, S., Lexcellent, C., 1996. A general macroscopic description of the thermomechanical behavior of shape memory alloys. Journal of the Mechanics and Physics of Solids 44 (6), 953–957.
Levitas, V.I., Ozsoy, I.B., 2009a. Micromechanical modeling of stress-induced phase transformations. Part 1. Thermodynamics and kinetics of coupled interface propagation and reorientation. International Journal of Plasticity 25 (2), 239–280.
Levitas, V.I., Ozsoy, I.B., 2009b. Micromechanical modeling of stress-induced phase transformations. Part 2. Computational algorithms and examples. International Journal of Plasticity 25 (3), 546–583.
Levitas, V.I., Stein, E., 1997. Simple micromechanical model of thermoelastic martensitic transformations. Mechanics Research Communications 24 (3), 309–318.
Lexcellent, C., Goo, B.C., Sun, Q.P., Bernardini, J., 1996. Characterization, thermomechanical behaviour and micromechanical-based constitutive model of shape-memory Cu–Zn–Al single crystals. Acta Materialia 44 (9), 3773–3780.
Lim, T.J., McDowell, D.L., 1999. Mechanical behavior of an Ni–Ti shape memory alloy under axial-torsional proportional and nonproportional loading. Journal of Engineering Materials and Technology 121, 9–18.
Luig, P., Bruhns, O., 2008. On the modeling of shape memory alloys using tensorial internal variables. Materials Science and Engineering A, 379–383.
Moumni, Z., Zaki, W., Nguyen, Q.S., 2008. Theoretical and numerical modeling of solid-solid phase change: Application to the description of the thermomechanical behavior of shape memory alloys. International Journal of Plasticity 24 (4), 614–645.
Muller, C., Bruhns, O., 2006. A thermodynamic finite-strain model for pseudoelastic shape memory alloys. International Journal of Plasticity 22 (9), 1658–1682.
Otsuka, K., Wayman, C.M., 1998. Shape Memory Materials. Cambridge University Press, Cambridge.
Pan, H., Thamburaja, P., Chau, F., 2007. Multi-axial behavior of shape-memory alloys undergoing martensitic reorientation and detwinning. International Journal of Plasticity 23 (4), 711–732.
Panico, M., Brinson, L., 2007. A three-dimensional phenomenological model for martensite reorientation in shape memory alloys. Journal of the Mechanics and Physics of Solids 55 (11), 2491–2511.
Patoor, E., Lagoudas, D.C., Entchev, P.B., Brinson, L.C., Gao, X., 2006. Shape memory alloys. Part I: General properties and modeling of single crystals. Mechanics of Materials 38 (5–6), 391–429.
Peng, X., Pi, W., Fan, J., 2008. A microstructure-based constitutive model for the pseudoelastic behavior of NiTi SMAs. International Journal of Plasticity 24 (6), 966–990.
Popov, P., Lagoudas, D.C., 2007. A 3-D constitutive model for shape memory alloys incorporating pseudoelasticity and detwinning of self-accommodated martensite. International Journal of Plasticity 23 (10–11), 1679–1720.
Raniecki, B., Lexcellent, C., 1998. Thermodynamics of isotropic pseudoelasticity in shape memory alloys. European Journal of Mechanics - A/Solids 17 (2), 185–205.
Reese, S., Christ, D., 2008. Finite deformation pseudo-elasticity of shape memory alloys – constitutive modelling and finite element implementation. International Journal of Plasticity 24 (3), 455–482.
Simo, J.C., Hughes, T.J.R., 1998. Computational Inelasticity. Springer-Verlag, New York.
Sittner, P., Hara, Y., Tokuda, M., 1995. Experimental study on the thermoelastic martensitic transformation in shape memory alloy polycrystal induced by combined external forces. Metallurgical and Materials Transactions A 26, 2923–2935.
Souza, A.C., Mamiya, E.N., Zouain, N., 1998. Three-dimensional model for solids undergoing stress-induced phase transformations. European Journal of Mechanics A/Solids 17 (5), 789–806.
Sun, Q.P., Hwang, K.C., 1993a. Micromechanics modelling for the constitutive behavior of polycrystalline shape memory alloys – I. Derivation of general relations.. Journal of the Mechanics and Physics of Solids 41 (1), 1–17.
Sun, Q.P., Hwang, K.C., 1993b. Micromechanics modelling for the constitutive behavior of polycrystalline shape memory alloys – II. Study of the individual phenomena. Journal of the Mechanics and Physics of Solids 41 (1), 19–33.
Thamburaja, P., 2005. Constitutive equations for martensitic reorientation and detwinning in shape-memory alloys. Journal of the Mechanics and Physics of Solids 53 (4), 825–856.
Thamburaja, P., Anand, L., 2002. Superelastic behavior in tension–torsion of an initially-textured Ti–Ni shape-memory alloy. International Journal of Plasticity 18 (11), 1607–1617.
Thamburaja, P., Pan, H., Chau, F., 2009. The evolution of microstructure during twinning: constitutive equations, finite-element simulations and experimental verification. International Journal of Plasticity. doi:10.1016/j.ijplas.2009.02.004.
Thiebaud, F., Lexcellent, C., Collet, M., Foltete, E., 2007. Implementation of a model taking into account the asymmetry between tension and compression, the temperature effects in a finite element code for shape memory alloys structures calculations. Computational Materials Science 41 (2), 208–221.
Van Humbeeck, J., 1999. Non-medical applications of shape memory alloys. Materials Science and Engineering A, 134–148.
Xiao, H., Bruhns, O.T., Meyers, A., 2006. Elastoplasticity beyond small deformations. Acta Mechanica 182 (1), 31–111.